Theory of nonlocal soliton interaction in nematic liquid crystals

Per Dalgaard Rasmussen and Ole Bang
COM•DTU Department of Communications, Optics & Materials, Technical University of Denmark, 2800 Kongens Lyngby, Denmark

Wieslaw Królikowski
Laser Physics Centre, Research School of Physical Sciences and Engineering, The Australian National University, Canberra, ACT 0200, Australia

(Received 10 June 2005; published 20 December 2005)

We investigate interactions between spatial nonlocal bright solitons in nematic liquid crystals using an analytical ("effective particle") approach as well as direct numerical simulations. The model predicts attraction of out-of-phase solitons and the existence of their stable bound state. This nontrivial property is solely due to the nonlocal nature of the nonlinear response of the liquid crystals. We further predict and verify numerically the critical outwards angle and degree of nonlocality which determine the transition between attraction and repulsion of out-of-phase solitons.

DOI: 10.1103/PhysRevE.72.066611 PACS number(s): 42.65.Tg, 42.65.Ky, 42.65.Sf

I. INTRODUCTION

Solitons arise in many different branches of science, including plasma physics, hydrodynamics, superconductivity, matter waves, and optics [1]. They are characterized by their ability to propagate over long distances and interact while preserving their shape. For many years propagation of optical spatial solitons has been widely studied in Kerr-like media with an intensity-dependent refractive index, which gives rise to the local nonlinear Schrödinger (NLS) equation [2].

In Ref. [3] Snyder and Mitchell studied a theoretical model for light propagation in a highly nonlocal medium, i.e., a medium where the change of the refractive index depends on the total power of the light beam instead of the local intensity. Using this assumption they reduced the problem to the linear equation for the harmonic oscillator. Interestingly, it turns out that the nematic liquid crystals (NLCs) exhibit such a high degree of nonlocality [4]. The strong nonlocality of NLC arises because of elastic forces between the liquid crystal molecules which act as a diffusion mechanism [5,6]. In early studies of light propagation in NLC the light intensities necessary to observe self-focusing were so high, that the thermal effects arising because of heating could not be neglected [7,8]. By applying a transverse electric field over the cell containing the NLC, the power required to observe propagation of stable self-focused structures can be lowered significantly [9]. More recent studies of localized structures in NLC include both experimental observations [10,11] and theoretical models [4,12]. See Ref. [13] for a review of soliton propagation in voltage biased cells containing NLC.

Other examples of systems where nonlocality plays a similar role are seen in different areas of nonlinear science, such as Bose-Einstein condensates [14] and plasmas [15]. In all these cases the underlying governing equation is the nonlocal NLS equation, which displays several nontrivial generic features, independent of the specific nature of the nonlocal response (see Refs. [16,17] for a review). In Ref. [18] nonlocality was shown to prevent the nonphysical collapse of beams after a finite propagation distance, which is predicted when using the local NLS equation. Nonlocality has also been shown to promote modulational instability in a defocusing Kerr medium [19,20], and may even accurately describe parametric wave interaction [21,22]. Furthermore, in Ref. [4] it was shown that nonlocal solitons in NLC have the same profiles as quadratic solitons. An interesting consequence of nonlocality is an attraction of dark solitons, that was predicted theoretically in Ref. [23] and has recently been demonstrated experimentally [24]. Nonlocality also allows the existence of stable ring vortex solitons [25].

Interaction between nonlocal bright solitons has also been shown to exhibit remarkable features, such as an attraction of out-of-phase bright solitons [26], and the existence of bound states consisting of two out-of-phase bright solitons [12,27]. Such results are a direct consequence of the nonlocality, since neither attraction nor bound states of dark solitons and out-of-phase bright solitons can occur in a local medium.

Nonlocal soliton interaction in NLC has previously been studied theoretically in (1+2)D using numerical methods [28]. In the present study we give the first analytical treatment of interactions between (1+1)D nonlocal bright solitons. We show that there is a critical degree of nonlocality above which out-of-phase solitons attract. These results are verified by direct numerical simulations. We further find bound states of out-of-phase bright solitons and the power threshold for their existence.

II. GOVERNING EQUATIONS

We study a simplified model for light propagation in a cell containing a liquid crystal in the nematic phase. The real physical model is naturally a three-dimensional model. Here we are interested in studying the qualitative physical characteristics of soliton interactions analytically, therefore we consider only one transversal dimension, as it has earlier been done in theoretical studies of modulational instability in NLC [29]. An external quasistatic electric field E_{LF} is applied

in the transverse dimension, in order to ensure that the field strength is above the Freèdericksz threshold, below which no reorientation occurs. Using the slowly varying envelope approximation for the evolution of the optical field $[A(X,Z)]$ and assuming a pretilt angle of $\pi/4$ in order to maximize the nonlinear response [5], we obtain the following NLS-type equation for A:

$$2ikA_Z + A_{XX} + \frac{k_0^2}{\epsilon_0}\Delta\epsilon_{HF}\Psi A = 0, \tag{1}$$

where $\Psi(X,Z)$ is the reorientation angle of the liquid crystal molecules due to the presence of the optical field. k_0 and k are the wave numbers in vacuum and in the liquid crystal, respectively. $\Delta\epsilon_{HF}$ is the anisotropy of the liquid crystal at the optical frequency and ϵ_0 is the vacuum permittivity. The governing equation for $\Psi(X,Z)$ is found by minimizing the internal energy of the liquid crystal due to deformations [[6], Sec. 6.3] and making a series expansion around a total reorientation angle of $\pi/4$. Under these assumptions the equation for Ψ is [4]

$$K\Psi_{ZZ} + K\Psi_{XX} - \frac{2\Delta\epsilon_{LF}E_{LF}^2}{\pi}\Psi + \frac{\Delta\epsilon_{HF}|A|^2}{4} = 0, \tag{2}$$

where $\Delta\epsilon_{LF}$ is the anisotropy of the liquid crystal at the frequency of the quasistatic electric field. K is the elastic constant of the liquid crystal, taken to be the same for twist, splay, and bend deformations. The system of Eqs. (1) and (2) is normalized by scaling the transverse coordinate with the width of the input beam ($x=X/X_0$), and the propagation coordinate with the diffraction length $z=Z/L_D$. Here X_0 represents the full width at half maximum (FWHM) of the amplitude of the input beam, and the diffraction length is given by $L_D=2kX_0^2$. Further, the fields A and Ψ are scaled as $a=A/A_0$ and $\psi=\Psi/\Psi_0$, where

$$A_0 = \frac{2E_{LF}}{\Delta\epsilon_{HF}k_0X_0}\sqrt{\frac{\epsilon_0\Delta\epsilon_{LF}}{\pi}}, \tag{3}$$

$$\Psi_0 = \frac{\epsilon_0}{k_0^2X_0^2\Delta\epsilon_{HF}}. \tag{4}$$

With these definitions we obtain the dimensionless equations:

$$ia_z + a_{xx} + \psi a = 0, \tag{5}$$

$$\epsilon\sigma^2\psi_{zz} + \sigma^2\psi_{xx} - \psi + \tfrac{1}{2}|a|^2 = 0, \tag{6}$$

where σ is the degree of nonlocality, defined as

$$\sigma^2 = \frac{\pi K}{2X_0^2E_{LF}^2\Delta\epsilon_{LF}}. \tag{7}$$

$\epsilon=1/(4X_0^2k^2)$ is a small parameter. Taking typical values for material parameters of the liquid crystal E7 [[6], Chap. 3] ($K=10^{-11}$ N, $\Delta\epsilon_{HF}=0.64\epsilon_0$, and $\Delta\epsilon_{LF}=15\epsilon_0$), and using a beam width of $X_0=10\ \mu$m and a field strength $E_{LF}=10^4$ V/m, which are common experimental values [10], we find $\sigma\approx5$, which corresponds to a rather strong nonlocality. For wavelengths in the visible and near infrared region (i.e., from 500 to 1500 nm) ϵ ranges from 10^{-6} to 10^{-5}. The diffraction length L_D is of the order of 1 mm.

Notice that σ can also be scaled out of the governing equations (5) and (6), by scaling the x and z coordinate with σ and σ^2, respectively ($x\to\sigma x$ and $z\to\sigma^2 z$), and scaling the fields a and ψ with σ^{-1} and σ^{-2}, respectively ($a\to\sigma^{-1}a$ and $\psi\to\sigma^{-2}\psi$), and finally redefining $\epsilon/\sigma^2\to\epsilon$. However, since we are interested here in comparing identical systems with different degrees of nonlocality, and because K is the physical parameter that is responsible for nonlocality, we have chosen the K-independent scaling parameters as described above.

It can be shown that the systems (5) and (6) can be derived from the variational principle with the following Lagrangian density

$$\mathcal{L} = -\mathrm{Im}\{a^*a_z\} - |a_x|^2 - \sigma^2\psi_x^2 - \psi^2 + |a|^2\psi - \epsilon\sigma^2\psi_z^2. \tag{8}$$

From this Lagrangian three integrals of motion can be obtained: the power P, the momentum M, and the Hamiltonian H, given by the expressions

$$P = \int_{-\infty}^{\infty}|a|^2\,dx, \tag{9}$$

$$M = \int_{-\infty}^{\infty}(\mathrm{Im}\{aa_x^*\} - 2\epsilon\sigma^2\psi_z\psi_x)dx, \tag{10}$$

$$H = \int_{-\infty}^{\infty}(|a_x|^2 + \sigma^2\psi_x^2 + \psi^2 - |a|^2\psi - \epsilon\sigma^2\psi_z^2)dx. \tag{11}$$

With the scaling used here, the physical power density becomes $\mathcal{P}=\frac{1}{2}(k/k_0)\epsilon_0cA_0^2X_0P$, where c is the speed of light. Using the parameter values from above we find $\mathcal{P}\approx50$ mW/m for $P=1$.

Here we study interactions between solitons in (1+1)D. Neglecting the term proportional to ϵ in Eq. (6), we can express ψ in terms of the intensity $I=|a|^2$ of the optical field. Using Fourier transformation and the convolution theorem we find

$$\psi(x,z) = \frac{1}{2}\int_{-\infty}^{\infty}R(x-x')I(x')dx', \tag{12}$$

where the normalized response function of the liquid crystal is given by

$$R(x) = \frac{1}{2\sigma}\exp\left(-\frac{|x|}{\sigma}\right). \tag{13}$$

For large σ the nonlocality is strong, and the response function becomes very wide. For small σ the response is almost local. In the limit $\sigma\to0$ the response function becomes a δ function, and we end up with the standard NLS equation for the evolution of a.

III. STATIONARY BRIGHT SOLITON SOLUTIONS

Ground state bright soliton solutions of Eqs. (5) and (6) have the form $a(x,z)=V(x;\lambda)\exp(i\lambda z)$ and $\psi(x,z)=W(x;\lambda)$,

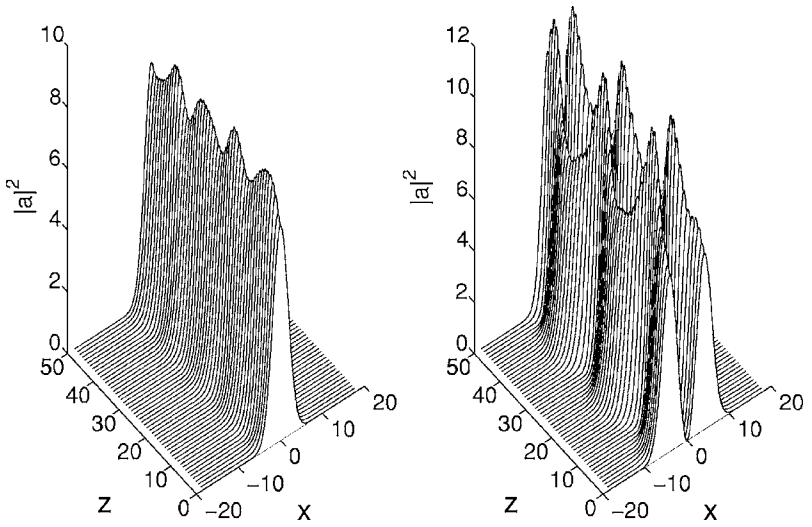

FIG. 1. Propagation of perturbed stationary profiles of a one hump soliton (left) and a bound state of two solitons (right). In both cases $\lambda=1$ and $\sigma=5$.

where the propagation constant λ is positive to ensure that the profiles of V and W decay monotonically to zero, as is the signature of the ground state. The profiles are found by solving the system

$$-\lambda V + V_{xx} + VW = 0, \tag{14}$$

$$\sigma^2 W_{xx} - W + \tfrac{1}{2}V^2 = 0, \tag{15}$$

subject to the boundary conditions $V, W \to 0$ for $x \to \pm\infty$. The numerical solutions of Eqs. (14) and (15) are well known [30–32]. Here we are interested in two types of bright soliton solutions, the fundamental (single hump solitons) as shown in Fig. 2, and bound states consisting of two out-of-phase bright solitons as shown in Fig. 5. These solutions are found numerically using a shooting method [[33], Sec. 16.1].

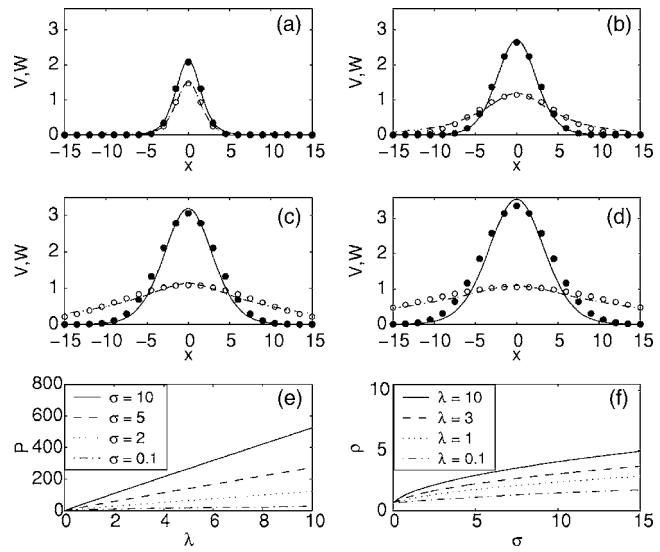

FIG. 2. Characteristics of ground state bright solitons of Eqs. (14) and (15). Plots (a)–(d) show solutions for $\lambda=1$ and different degrees of nonlocality: $\sigma=1$ (a), $\sigma=5$ (b), $\sigma=10$ (c), and $\sigma=15$ (d). The lines show the exact numerical profiles (solid, V; dashed, W). Approximate variational solution is also shown (points, V; circles, W). (e) shows the power versus λ and (f) shows the waist ratio $\rho=b_2/b_1 \geqslant 1/\sqrt{2}$ versus nonlocality for the solutions found using the Gaussian profiles.

The stability of both types of solutions is examined by solving Eqs. (5) and (6) numerically for $\epsilon=0$ with perturbed stationary profiles as initial conditions. The perturbed profiles used here are the profiles found using the approximate variational and effective particle approach discussed in the next section. Both types of solutions oscillate due to the perturbation, but maintain their profile over 50 diffraction lengths as illustrated in the examples shown in Fig. 1. Extensive numerical simulations confirm stability and robustness of these solitons in all cases considered.

Exact analytical solutions are only known to exist for the two special cases when $\lambda\sigma^2=1$ and when $\sigma=0$. When $\lambda\sigma^2=1$, V, and W become proportional to each other, and Eqs. (14) and (15) reduce to a single equation. The bright soliton solution found first, in Ref. [34] is $W(x)=\sqrt{\lambda/2}V=3\lambda/2\ \mathrm{sech}^2(\sqrt{\lambda}x/2)$. When $\sigma=0$ we have the standard NLS equation, where the bright soliton solution is $W=V^2/2=2\lambda\ \mathrm{sech}^2(\sqrt{\lambda}x)$. In the weakly and highly nonlocal region various approximations can be made to simplify the equations, and exact analytical solutions to these simplified equations can be found as discussed in Refs. [21,35].

Equations (5) and (6) are Galilean invariant, i.e., from the stationary solutions $V(x;\lambda)$ and $W(x;\lambda)$ of Eqs. (14) and (15), we can construct solutions of Eqs. (5) and (6) moving with transverse velocity v. This is done using the transformation

$$a(x,z) = \pm\frac{1}{\sqrt{1+v^2\epsilon}}V\left(\frac{1}{\sqrt{1+v^2\epsilon}}(x-x_0-vz);\lambda\right) \times \exp\left(i\left[\frac{v}{2}x + \frac{4\lambda - v^2 - v^4\epsilon}{4(1+v^2\epsilon)}z\right]\right), \tag{16}$$

$$\psi(x,z) = \frac{1}{1+v^2\epsilon}W\left(\frac{1}{\sqrt{1+v^2\epsilon}}(x-x_0-vz);\lambda\right), \tag{17}$$

where x_0 is an arbitrary constant. Notice that Eqs. (16) and (17) are exact for all values of ϵ. We see that for $\epsilon=0$ the

usual Galilean invariance of the NLS equation is recovered. The effect of the ϵ term is to decrease the amplitude and increase the width of the moving solutions, compared to their stationary profiles.

Instead of solving Eqs. (14) and (15) numerically we can approximate the stationary profiles $V(x;\lambda)$ and $W(x;\lambda)$ using a variational approach [31]. Inserting Gaussian trial functions $V(x;\lambda)=a_1\exp(-x^2/b_1^2)$ and $W(x;\lambda)=a_2\exp(-x^2/b_2^2)$ in the Lagrangian density (8) and integrating over the transverse dimension, we find the reduced Lagrangian. The global minimum of the reduced Lagrangian is found by varying with respect to the amplitudes and widths (a_1, a_2, b_1, and b_2). This leads to the following expressions for these quantities:

$$a_1 = 2(2\rho^2+1)^{3/2}\sqrt{\frac{\lambda}{\rho(4\rho^2+1)(2\rho^2+3)}}, \tag{18}$$

$$a_2 = \sqrt{2}\frac{\lambda(2\rho^2+1)^{3/2}}{\rho(4\rho^2+1)}, \tag{19}$$

$$b_1 = \sqrt{\frac{4\rho^2+1}{\lambda}}, \tag{20}$$

$$b_2 = \rho b_1, \tag{21}$$

$$\sigma = \rho\sqrt{\frac{(4\rho^2+1)(2\rho^2-1)}{\lambda(2\rho^2+3)}}, \tag{22}$$

where the waist ratio $\rho=b_2/b_1$ has been introduced. We see that we cannot express everything in terms of the system parameters λ and σ, without using the explicit formula for finding the roots of a third degree polynomial. Instead we solve Eq. (22) numerically. It can be shown that for given $\lambda,\sigma\geqslant 0$ Eq. (22) has only one positive solution $\rho\geqslant 1/\sqrt{2}$. Hence the variational method determines the amplitudes and widths of a and ψ uniquely for given values of λ and σ. In Fig. 2 exact numerical solutions are plotted together with the corresponding variational approximation for $\lambda=1$ and different values of σ. We see that the two solutions agree well in the region near the soliton peak. Deviations occur in the tails of the solitons, which is a direct consequence of our Gaussian ansatz. The tail dynamics of the exact solution is found by neglecting the nonlinear terms in Eqs. (14) and (15). Solving the decoupled system we see that the tails are exponentially decaying functions $V(x;\lambda)\propto\exp(-\sqrt{\lambda}|x|)$ and $W(x;\lambda)\propto\exp(-|x|/\sigma)$. The exact behavior of the soliton tails is therefore different from the behavior of our Gaussian ansatz.

Also in Fig. 2 the power ($P=\sqrt{\pi/2}a_1^2b_1$) of the trial function is plotted as a function of λ. The plot indicates that the ground state solitons are stable, since $dP/d\lambda>0$, which is a necessary condition for stability [36]. In addition, in Fig. 2 the waist ratio $\rho=b_2/b_1$ is plotted as a function of nonlocality. The plot shows that in the highly nonlocal region ($\sigma\gg 1$) we have always $\rho\gg 1$, which again shows that in this region the change in the refractive index extends far beyond the optical field.

IV. SOLITON BOUND STATES

In the following we consider interactions between stationary bright solitons for the system Eqs. (5) and (6) when neglecting the term proportional to ϵ. Inclusion of this term introduces a singular perturbation, which appears to be very difficult to handle both analytically and numerically. A superposition of two solitons with identical profiles separated by $2x_0$, and with opposite transverse velocities ($\pm v$) is substituted into the Lagrangian density (8) without the ϵ term. If we only consider solitons in phase or with a phase difference of π, we can assume symmetric interaction, i.e., there can be no transfer of energy between the solitons. To proceed further we apply the method described in Refs. [37,38] and further developed in Ref. [39] for nonzero initial velocities. Introducing a slow propagation variable ($z_1=\mu z, \mu\ll 1$), and assuming that the soliton phase and position vary adiabatically through z_1, we can reduce the governing equations to the problem of a particle moving in an external potential ("effective particle approach"). To the first order in μ the dynamics of this particle is described by the following Lagrangian:

$$L = \tfrac{1}{2}P(\lambda)v^2 - U(\lambda,\sigma,x_0,v,\theta), \tag{23}$$

where θ is the phase difference between the solitons ($\theta=0$ or π) and P is the power of each soliton. U represents an interaction potential, and is given by

$$U = -\int [\pm 2V_1V_2W_1\cos(vx) + V_1^2W_2]dx, \tag{24}$$

where $V_1=V(x-x_0;\lambda)$ and $V_2=V(x+x_0;\lambda)$ are stationary profiles with peaks at $\pm x_0$; W_1 and W_2 are defined similarly. The plus sign in Eq. (24) is for solitons in phase ($\theta=0$) and the minus sign is for solitons with a phase difference of $\theta=\pi$.

A remarkable fact about nonlocal bright solitons is that solitons with a phase difference of π can attract each other if the nonlocality is strong enough, as shown numerically in Ref. [21] and experimentally in Ref. [26]. This is never the case in a local medium, where bright solitons with a phase difference of π always repel. An attraction of two out-of-phase bright nonlocal solitons can be understood in the following way: Light is confined in regions with a high refractive index. In the middle between the two peaks, the intensity will be zero, but the optically induced change in the refractive index is not zero because of the nonlocality. As shown in Fig. 5, the induced change in the refractive index is almost maximal at the midpoint between the intensity peaks, when the nonlocality is strong ($\sigma\gg 1$).

Indeed, the structure of the potential (24) does predict a bound state of two out-of-phase solitons, as shown in Fig. 3, where the potential (24) is plotted as a function of peak separation for $\lambda=1$ and $\sigma=10$. We see that when using the Gaussian profiles the potential has the same qualitative shape as when using the exact profiles. In both cases the potential is attractive for large separations and repulsive for small separations. For $x_0\approx 5.4$ we have $dU/dx_0=0$, which corresponds to a bound state, where the strength of the attractive and repulsive forces acting on the soliton have the same magni-

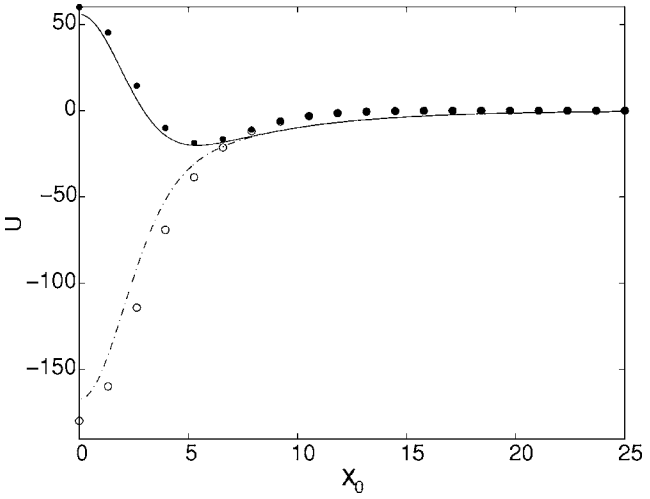

FIG. 3. Interaction potential U as a function of peak separation found with Eq. (24) with $\lambda=1$, $\sigma=10$, and $v=0$. Lines show potential when using exact numerical profiles (dash-dotted line, solitons in-phase; solid line, phase difference of π). Points show the potential when using the Gaussian approximation for the profiles (○, in-phase and ●, phase difference π).

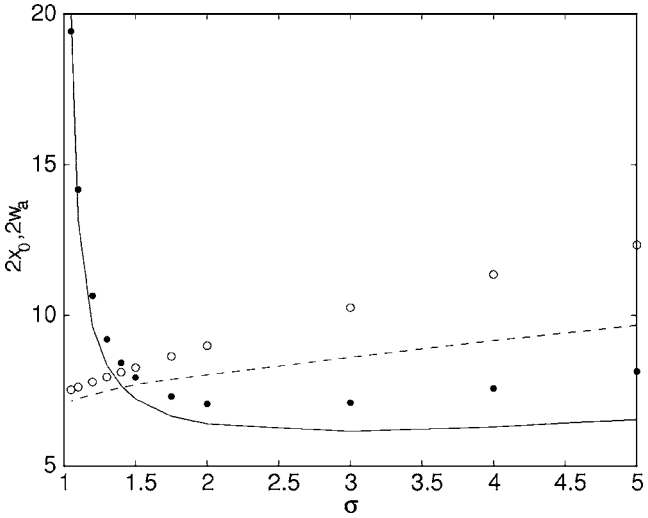

FIG. 4. Peak separation ($2x_0$) in a bound state of two out-of-phase solitons for $\lambda=1$. The solid line shows the numerically found exact peak separation and dots (●) represent values predicted by Eq. (25). The dashed line shows the width ($2w_a$) of one of the solitons found numerically; the circles (○) shows $2w_a$ as predicted by the effective particle approach with the Gaussian solitons.

tude. In Fig. 3 the same potential, but now for in-phase solitons is also plotted. Here we see that dU/dx_0 is always positive, which means that two in-phase initially parallel nonlocal solitons will always collide. Inserting the Gaussian approximations for the solitons in the potential (24) and solving the equation $dU/dx_0=0$ for x_0 with $v=0$ gives

$$x_0 = \frac{1}{2}\sqrt{\frac{(8\rho^4+6\rho^2+1)\ln(\rho^2+1)}{\lambda(\rho^2-1)}}. \tag{25}$$

We see that the perturbative analysis predicts that a bound state only exists when $\rho>1$. Using Eq. (22) one finds that this corresponds to $\lambda\sigma^2>1$. Relating this to the physically measurable quantities the power P and width b_1, we find the requirement $b_1P>\sqrt{2\pi}\times 54/5\approx 27.1$, when using the Gaussian approximation. The criterion $\lambda\sigma^2>1$ for the existence of a bound state was also found when solving the equations numerically. In other words, the bound state only exists for a sufficiently large degree of nonlocality $\sigma>1/\sqrt{\lambda}$ or correspondingly a sufficiently high power $P>27.1/b_1$. Fixing the width of the input beam to be X_0, means $b_1=1$. In this case the threshold power for the existence of a bound state is $P=27.1$, corresponding to $\mathcal{P}=1.4$ mW/mm for the physical parameter values given in Sec. II.

The separation in a bound state found numerically is shown in Fig. 4, together with the separations found with Eq. (25). The separations predicted by the perturbative analysis are consistent with the results found numerically. Both results indicate that $x_0\to\infty$ for $\lambda\sigma^2\to 1$. In other words, when the nonlocality is too weak ($\sigma\to 1/\sqrt{\lambda}$), the solitons are so far apart that they cannot "feel" each other, and the state cannot be regarded as a bound state anymore. Furthermore, both approaches predict a local minimum around $\sigma=3$ for the case $\lambda=1$. In Fig. 4 two times the exact width of one of the solitons in the bound state is also plotted. We see that the widths found numerically are consistent with the widths predicted by our perturbative approach. The perturbative result is most accurate when the separations are larger than the soliton width. This is to be expected since the analytical approach relies on the assumption of weak soliton interaction.

In Fig. 5 profiles of the bound states found numerically by solving Eqs. (14) and (15) are plotted together with the approximations found using the effective particle approach with the Gaussian approximate profiles. The plots show that the approximate results are in good qualitative agreement with the exact ones, found numerically, in both weakly local and highly nonlocal regimes. Again we see that the best

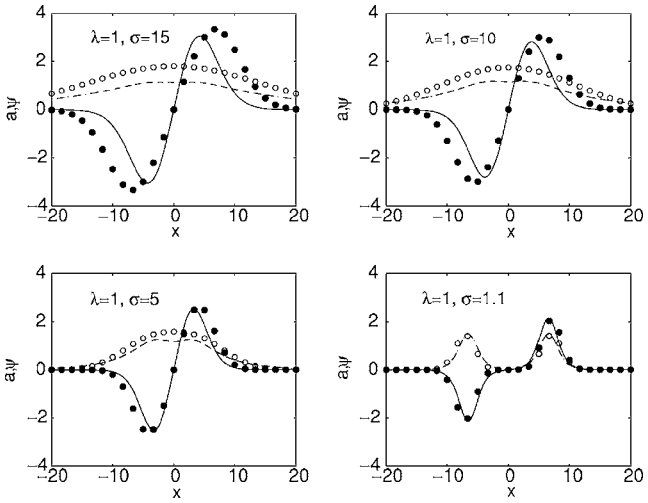

FIG. 5. Examples of bound states found numerically for $\lambda=1$ (a, line; ψ, dash-dotted line). Also the bound states predicted by the effective particle approach using the approximate Gaussian profiles are shown (a, points; ψ, circles).

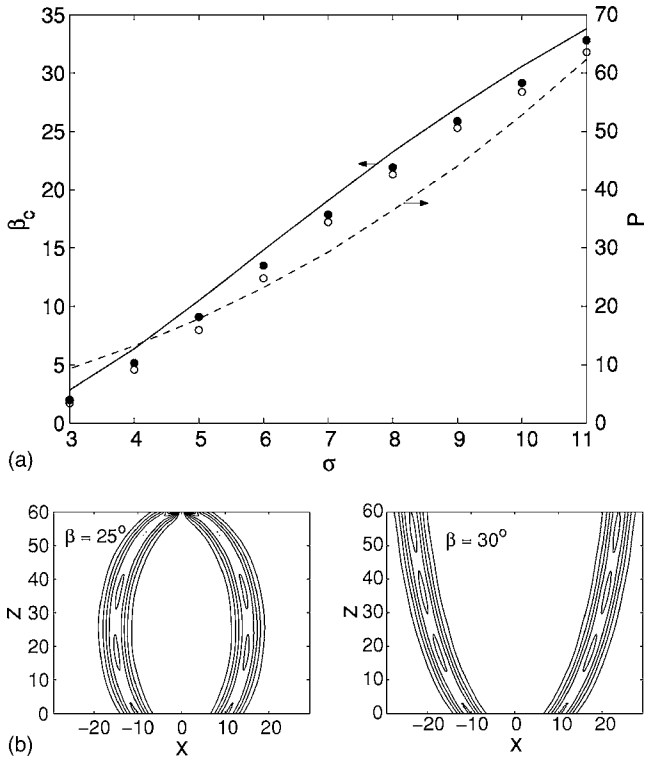

FIG. 6. Escape angle (β_c) in degrees versus nonlocality for out-of-phase solitons, width $w_a=6.9$ and separation $2x_0=3w_a$. The solid line shows the escape angle calculated using the effective particle approach. Numerical simulations where the solitons continued to move apart after 60 diffraction lengths are marked with a ●, and simulations where they began to move towards each other are marked with a ○. The dashed line shows the power (P) of each of the solitons. Below two examples are shown, one where the solitons do not escape, and one where they, after 60 diffraction lengths, still move away from each other. These simulations are for $P=62.3$ and $\sigma=10$.

quantitative agreement is found in the weakly nonlocal region, where the separations are highest, when compared to the individual soliton width. In Fig. 1 we have already shown that the bound state can be stable, which we found to be the case in all our simulations.

V. SOLITON INTERACTION

In this section we will use the Lagrangian given in Eq. (23) to determine the outcome of the interaction of two ground state bright solitons launched with a small relative angle, so they move initially at diverging trajectories. As the total energy $E_{\mathrm{tot}}=\frac{1}{2}Pv^2+U$ is conserved, this quantity can be used to determine whether or not the "effective particle" (the soliton) is trapped by the potential. If the energy is greater than 0, the particle can escape from the potential barrier, i.e., the two solitons will keep moving away from each other. If the total energy is negative the particle is trapped by the potential, i.e., the two solitons will propagate together, with their separation exhibiting periodic oscillations. Using the potential (24) we can predict the escape velocity, which is the velocity where the total energy is 0. Here we cannot use

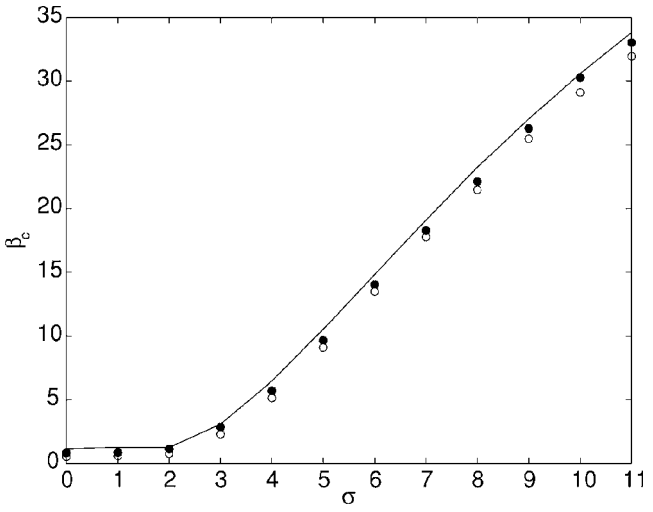

FIG. 7. Escape angle (β_c) in degrees as a function of nonlocality for in-phase solitons. The parameters are the same as those in Fig. 6.

the Gaussian approximations for the soliton profiles since the interaction for large separations is dependent on the soliton tails, but the tail of the exact profile is different from a Gaussian as discussed earlier. Therefore we find the escape velocity numerically by solving

$$\tfrac{1}{2}Pv_c^2+U=0, \tag{26}$$

where v_c is the escape velocity. U and P are evaluated using the numerically found exact profiles. In Fig. 6 the escape angle $\beta_c=\tan^{-1}v_c$ is plotted as a function of the degree of nonlocality for solitons out of phase ($\theta=\pi$). Notice that because of different normalization parameters in the x and z direction, the physical escape angle is given by $\beta_c^*=\tan^{-1}(v_cX_0/L_D)$. The width of the optical field is kept constant ($w_a=6.9$) and the soliton peak separation is also constant ($2x_0=3w_a$) to ensure small initial overlap between the solitons for all degrees of nonlocality, since this is the requirement for our adiabatic theory to work. We see that the effective particle approach enables us to give a good estimate of the escape velocity, although the effective particle approach tends to slightly overestimate the escape angle. For the soliton parameters used in this experiment $\sigma\approx 3$ is the critical value of the nonlocality, below which out-of-phase solitons no longer attract, even if launched in parallel. Therefore the plot for the escape angle in Fig. 6 does not extend below $\sigma=3$.

Interaction of in-phase solitons was also investigated. The results for the escape angle in the highly nonlocal regime were almost identical to those of the out-of-phase solitons as shown in Fig. 7. This agrees with experimental results of Peccianti *et al.* [26] where interactions between both out-of-phase and in-phase nematicons were investigated. The main qualitative difference in the interaction of nonlocal in-phase solitons and out-of-phase solitons, is the fact that for the in-phase solitons there always exists a finite escape angle for all values of $\sigma\geqslant 0$, indicating that, as it is well known, in-phase solitons always attract.

VI. CONCLUSION

We studied interactions between nonlocal spatial solitons using a perturbative analytical approach, as well as direct numerical simulations. Bound states consisting of two out-of-phase solitons were analytically described. The analytical results agree well with the exact numerical results for all degrees of nonlocality σ. The best quantitative results of the perturbative approach are found in the weakly nonlocal region. Both the perturbative approach and the numerical simulations indicate that a bound state solution of systems (14) and (15) exist for $\lambda\sigma^2 > 1$, where λ is the soliton eigenvalue. For a Gaussian input beam with power P and width b_1, we showed that this requirement approximately could be expressed as $b_1 P > 27.1$. Because of the scaling of the governing equations a physical initial beam width of X_0 corresponds to $b_1 = 1$, and the power threshold becomes $\mathcal{P} = 1.4$ mW/mm for typical parameter values.

Escape angles for solitons in phase and out of phase (phase difference π) are also predicted using the perturbative method. The results are found to be quantitatively consistent with numerical simulations of the full set of governing equations for all degrees of nonlocality. Here it was found that in-phase solitons always attract, while a certain degree of nonlocality is necessary for out-of-phase solitons to attract. This degree of nonlocality was shown to be equivalent to the criterion stated above for existence of a bound state.

ACKNOWLEDGMENT

W.K acknowledges support of the Australian Research Council.

[1] A. Scott, *Nonlinear Science: Emergence and Dynamics of Coherent Structures* (Oxford University Press, Oxford, 1999).
[2] G. I. Stegeman and M. Segev, Science **286**, 1518 (1999).
[3] A. W. Snyder and D. J. Mitchell, Science **276**, 1538 (1997).
[4] C. Conti, M. Peccianti, and G. Assanto, Phys. Rev. Lett. **91**, 073901 (2003).
[5] N. V. Tabiryan, A. V. Sukhov, and B. Ya Zel'dovich, Mol. Cryst. Liq. Cryst. **136**, 1 (1986).
[6] I. C. Khoo, *Liquid Crystals—Physical Properties and Nonlinear Optical Phenomena* (Wiley-Interscience, New York, 1995).
[7] E. Braun, L. P. Faucheux, and A. Libchaber, Phys. Rev. A **48**, 611 (1993).
[8] M. A. Karpierz, M. Sierakowski, M. Swillo, and T. Wolinsky, Mol. Cryst. Liq. Cryst. **320**, 157 (1998).
[9] M. Peccianti, A. De Rossi, G. Assanto, A. De Luca, C. Umeton, and I. C. Khoo, Appl. Phys. Lett. **77**, 7 (2000).
[10] C. Conti, M. Peccianti, and G. Assanto, Phys. Rev. Lett. **92**, 113902 (2004).
[11] J. Beeckman, K. Neyts, X. Hutsebaut, C. Cambournac, and M. Haelterman, Opt. Express **12**, 1011 (2004).
[12] D. W. McLaughlin, D. J. Muraki, and M. J. Shelley, Physica D **97**, 471 (1996).
[13] G. Assanto and M. Peccianti, IEEE J. Quantum Electron. **39**, 13 (2003).
[14] A. Parola, L. Salasnich, and L. Reatto, Phys. Rev. A **57**, R3180 (1998).
[15] A. G. Litvak, V. A. Mironov, G. M. Fraiman, and A. D. Yunakovskii, Sov. J. Plasma Phys. **1**, 31 (1975).
[16] W. Królikowski, O. Bang, N. I. Nikolov, D. Neshev, J. Wyller, J. J. Rasmussen, and D. Edmundson, J. Opt. B: Quantum Semiclassical Opt. **6**, S288 (2004).
[17] W. Królikowski, O. Bang, J. Wyller, and J. J. Rasmussen, Acta Phys. Pol. A **103**, 133 (2003).
[18] O. Bang, W. Królikowski, J. Wyller, and J. J. Rasmussen, Phys. Rev. E **66**, 046619 (2002).
[19] W. Królikowski, O. Bang, J. J. Rasmussen, and J. Wyller, Phys. Rev. E **64**, 016612 (2001).
[20] J. Wyller, W. Królikowski, O. Bang, and J. J. Rasmussen, Phys. Rev. E **66**, 066615 (2002).
[21] N. I. Nikolov, D. Neshev, O. Bang, and W. Z. Królikowski, Phys. Rev. E **68**, 036614 (2003).
[22] I. V. Shadrivov and A. A. Zharov, J. Opt. Soc. Am. B **19**, 596 (2002).
[23] N. I. Nikolov, D. Neshev, W. Królikowski, O. Bang, J. J. Rasmussen, and P. L. Christiansen, Opt. Lett. **29**, 286 (2004).
[24] A. Dreischuh, D. Neshev, D. E. Petersen, O. Bang, and W. Królikowski, e-print physics/0504003.
[25] D. Briedis, D. E. Petersen, D. Edmundson, W. Królikowski, and O. Bang, Opt. Express **13**, 435 (2005).
[26] M. Peccianti, K. A. Brzdakiewicz, and G. Assanto, Opt. Lett. **27**, 1460 (2002).
[27] X. Hutsebaut, C. Cambournac, M. Haelterman, A. Adamski, and K. Neyts, Opt. Commun. **233**, 211 (2004).
[28] A. Fratalocchi, M. Peccianti, C. Conti, and G. Assanto, Mol. Cryst. Liq. Cryst. **421**, 197 (2004).
[29] G. Assanto, M. Peccianti, and C. Conti, IEEE J. Sel. Top. Quantum Electron. **10**, 862 (2004).
[30] A. V. Buryak and Y. S. Kivshar, Phys. Lett. A **197**, 407 (1995).
[31] V. V. Steblina, Y. S. Kivshar, M. Lisak, and B. A. Malomed, Opt. Commun. **118**, 345 (1995).
[32] A. V. Buryak, P. Di Trapani, D. V. Skryabin, and S. Trillo, Phys. Rep. **370**, 63 (2002).
[33] W. H. Press, B. P. Flannery, S. A. Teukolsky, and W. T. Vetterling, *Numerical Recipes* (Cambridge University Press, Cambridge, 1989).
[34] Y. N. Karamzin and A. P. Sukhorukov, JETP Lett. **20**, 339 (1974) [Sov. Phys. JETP **41**, 414 (1976)].
[35] W. Królikowski and O. Bang, Phys. Rev. E **63**, 016610 (2001).
[36] M. G. Vakhitov and A. A. Kolokolov, Radiophys. Quantum Electron. **16**, 783 (1973).
[37] V. V. Steblina, Yu. S. Kivshar, and A. V. Buryak, Opt. Lett. **23**, 156 (1998).
[38] A. V. Buryak and V. V. Steblina, J. Opt. Soc. Am. B **16**, 245 (1999).
[39] S. K. Johansen, O. Bang, and M. P. Sørensen, Phys. Rev. E **65**, 026601 (2002).